

---

## Research Article

---

# Studying the Morphology of Lyophilized Protein Solids Using X-ray Micro-CT: Effect of Post-freeze Annealing and Controlled Nucleation

Ken-ichi Izutsu,<sup>1,3</sup> Etsuo Yonemochi,<sup>2</sup> Chikako Yomota,<sup>1</sup> Yukihiro Goda,<sup>1</sup> and Haruhiro Okuda<sup>1</sup>

Received 6 January 2014; accepted 14 May 2014; published online 31 May 2014

**Abstract.** The objective of this study was to determine how different techniques used during the freezing step of lyophilization affect morphology of the dried protein solids. Aqueous solutions containing recombinant human albumin, trehalose, and sodium phosphate buffer were dried after their freezing by shelf-ramp cooling, immersion in liquid nitrogen, or controlled ice nucleation. Some shelf-frozen solutions were heat treated (annealed) before the vacuum drying. We used three-dimensional (3D) X-ray micro-computed tomography (micro-CT) and scanning electron microscopy (SEM) to study the morphology of solids. The X-ray micro-CT images of the lyophilized microporous solids showed traces of varied size and structure ice crystals that were comparable to corresponding SEM images. A post-freeze heat treatment and a controlled nucleation both induced larger ice crystal ghosts in the solids. The variations in the structure of walls surrounding ice crystals, formed by the different freezing procedures, should affect the water vapor transition during the primary and secondary drying. Some solids also showed higher-density layer in the upper surface. Overall, the simple sample preparation procedures and the ample morphological information make the X-ray micro-CT appropriate for analyzing lyophilized pharmaceuticals.

**KEY WORDS:** annealing; controlled nucleation; freeze-drying; ice sublimation; X-ray micro-CT.

## INTRODUCTION

Freeze-drying is a popular method for formulating various biopharmaceuticals, vaccines, and molecular assembly drug delivery systems (e.g., liposomes) that are not sufficiently stable in aqueous solutions (1). The increasing clinical use of protein pharmaceuticals, particularly high-dose and high-concentration therapeutic antibody formulations, emphasizes the importance of optimizing this high-energy and time-consuming process (2–4). The lyophilization process is composed of three segments: freezing, ice sublimation (primary drying), and removing unfrozen water from solids (secondary drying). The primary drying step often takes a long time (e.g., several days) because of the low product temperatures involved in the process. Formation of ice-sublimated upper solid layer also perturbs transition of water vapor (i.e., product resistance) from the remaining frozen solution layer.

Optimizing formulations and processes are popular approaches to achieve efficient ice sublimation and high-quality-end products. Sublimation of ice occurs more rapidly at higher temperatures. Each frozen solution, however, has its own “highest allowable” temperature, above which the particular system risks losing its structural integrity, through either the collapse or the melt-back

phenomena during the primary drying step. These physical changes damage the quality of lyophilized formulations in various ways (e.g., unfavorable appearance, component crystallization, and higher residual water content). Since many lyophilized therapeutic protein and liposome formulations contain disaccharides (e.g., sucrose, trehalose) as amorphous stabilizer, controlling the lyophilization chamber pressure and the shelf temperature, such that the product is kept at a slightly lower temperature than its allowable product temperature (collapse temperature:  $T_c$ ) of the particular formulation, allows rapid ice sublimation without causing any physical changes in the solid phase. Thermal analysis of frozen solutions provides the glass transition temperature of the maximally freeze-concentrated solute phase ( $T_g'$ ), which is often used as a surrogate for  $T_c$ . The difference between  $T_c$  and  $T_g'$  becomes larger in higher-concentration protein solutions (5).

Some processes such as post-freeze heat treatment (annealing) and controlled nucleation have recently gained attention as methods that enable faster ice sublimation (6–10). Usual cooling of vials on lyophilizer shelves induces spontaneous freezing of aqueous solutions at different degrees of supercooling, resulting in large inter-vial and inter-batch variations in the ice crystal sizes and sublimation times. Exposing the frozen solutions to higher temperatures induces larger ice crystals by Ostwald ripening (10). The resulting large and continuous pores in the solid layer allow faster transition of water vapor during the primary drying. The post-freeze heat treatment has also been used to induce crystallization of some APIs (e.g., antibiotics) (2,11). Recent studies indicate that

<sup>1</sup> National Institute of Health Sciences, Setagaya, Tokyo 158-8501, Japan.

<sup>2</sup> Hoshi University, Shinagawa, Tokyo 142-8501, Japan.

<sup>3</sup> To whom correspondence should be addressed. (e-mail: izutsu@nihs.go.jp)

controlled ice nucleation, which triggers simultaneous ice formation at relatively high temperatures, confers larger ice crystals and thereby faster sublimation. Various controlled nucleation methods, including ultrasound (12,13), ice fog (14,15), vacuum-induced surface freezing (16), release of pressurized chamber (8,17), and release of depressurized chamber (18), have been reported. Better understanding of their effects on the product quality (e.g., morphology, stability, component crystallinity, ability to keep sterile conditions) should assist their application (19).

The morphology of lyophilized microporous solids, particularly the size and structure of the pores created during ice sublimation, provides valuable information about the water vapor pathways, the occurrence of physical collapses, and the consistency of the process (20). Optical microscopes and scanning electron microscopy (SEM) have been used to characterize the local architecture of freeze-dried solids, but the morphological information that can be attained by these conventional methods is limited to those at the cross-sectional surfaces. Moreover, sample preparation for SEM may alter the structure of microporous noncrystalline solids that are hygroscopic and physically unstable. Application of other analytical methods (e.g., scaffolds formed by resins or polymer matrix) is limited because of their complex sample preparation procedures (21–23).

The objective of this study was to elucidate the effects of post-freeze annealing and the controlled ice nucleation on the morphology of freeze-dried protein solids by 3D X-ray micro-computed tomography (micro-CT) and SEM. The X-ray micro-CT is a valuable method to characterize microporous structure of granules (24), particle packing (25), and compaction of powders (26) in pharmaceutical formulations. Some studies indicated that the X-ray micro-CT provides valuable information about the structure of ice crystals in frozen foods after their freeze-drying (27,28). This method has also been used to analyze morphology of some lyophilized tissue engineering scaffolds (29), lyophilized protein pharmaceuticals (20), or to monitor ice sublimation during the primary drying step (30). Availability of the local morphology inside the microporous solids should offer a distinct advantage of the method. Recent advances in the systems (e.g., X-ray source, detector, stage control, data processing) have significantly improved the spatial resolution of the resulting images (31–33).

## MATERIALS AND METHODS

### Materials

Recombinant human albumin (rHA) expressed in rice (Cellastim) and trehalose dihydrate were purchased from Sigma-Aldrich Co. (St Louis, MO). Monosodium and disodium hydrogen phosphate were obtained from Wako Pure Chemical Co. (Osaka, Japan). The rHA protein was dialyzed against a sodium phosphate buffer (20 mM, pH 7.0) overnight before lyophilization.

### Freeze-Drying

Freeze-drying was performed using a lyophilizer (FZ-6, Labconco Co., Kansas City, MO). Aqueous solutions (1.2 mL each) containing recombinant human albumin (20 mg/mL),

trehalose (50 mg/mL), and sodium phosphate buffer (20 mM, pH 7.0) in flat-bottom glass tubes (diameter 16 mm, height 24 mm, 24 tubes, FLAT Glass Co., Nagareyama, Japan) were transferred to the lyophilizer shelf and were frozen by cooling the shelf from room temperature to  $-32^{\circ}\text{C}$  at  $0.5^{\circ}\text{C}/\text{min}$  (shelf-ramp cooling). The depth of the solutions was approximately 7 mm. Thirty flat-bottomed borosilicate glass vials (21-mm diameter) containing the albumin and trehalose mixture solutions (2 mL) were applied for the freeze-drying with the tubes to reduce the effect of radiation heat transfer during the process. Primary drying was performed at  $-32^{\circ}\text{C}$  for 30 h (0.03 mbar) after the temperature of the shelf was kept at  $-32^{\circ}\text{C}$  for 2 h. For the secondary drying step, the lyophilizer shelf was heated to  $30^{\circ}\text{C}$  at  $0.2^{\circ}\text{C}/\text{min}$  and maintained at the temperature for 4 h (0.03 mbar). Nitrogen gas was introduced into the chamber to break the vacuum. The tubes were sealed outside of the lyophilizer. Thermocouples were used to monitor the temperature profiles inside of several vials.

Some of the shelf-frozen solutions ( $-32^{\circ}\text{C}$ , 2 h) underwent a post-freeze heat treatment at  $-10^{\circ}\text{C}$  for 2 h before vacuum drying at  $-32^{\circ}\text{C}$ . The temperature of the lyophilizer shelf was adjusted at  $0.5^{\circ}\text{C}/\text{min}$  before and after the heat treatment. Some solutions were frozen by immersing the tubes and vials in liquid nitrogen before they were transferred to the precooled lyophilizer shelf ( $-32^{\circ}\text{C}$ ,  $\text{LN}_2$ -freezing). For this study, a modified controlled ice nucleation method based on the one reported by Geidobler *et al.* was also applied in the freezing step of some protein solutions (18). For the controlled nucleation, the sample-loaded lyophilizer shelf was cooled from room temperature to  $-5^{\circ}\text{C}$  and maintained at that temperature for 1 h. Ice nucleation was triggered by a quick release of the vacuum after the chamber pressure was reduced to 4 mbar. Visual observation indicated simultaneous ice formation from the top of all solutions upon introduction of nitrogen gas through the drain. Primary drying was started after the shelf was cooled to  $-32^{\circ}\text{C}$  ( $0.5^{\circ}\text{C}/\text{min}$ ).

### 3D X-ray Micro-CT Analysis

3D X-ray micro-CT scans were performed using the TDM 1000 H-II (2k) system (Yamato Scientific Co., Tokyo, Japan) with a 40-kV (0.085 mA) microfocus X-ray source at Microscopic Scan Co. (Tokyo). The cylindrical freeze-dried cakes were placed inversely on a polystyrene foam cube inserted between the cake and the rotating stage and were adhered to the cube with double-sided tape. A carbon tool steel blade precision knife was used to prepare cubic pieces (2–3 mm each side) from inside of the dried solids. These solids were used to obtain smaller field-of-view images. Samples were scanned in an atmospheric environment. X-ray shadow images were acquired in the dimensions of 1.0 to 17.0 mm per side; 1,000–1,500 views; and 5–15 frames per view, with a pixel resolution of 0.5 to 8  $\mu\text{m}$  (approximately 20-min scan). The X-ray shadow images were reconstructed into 3D cross sections using a VGStudio MAX 2.1 program (Volume Graphics GmbH, Heidelberg, Germany), and all subsequent analyses were based on the volume data set. Quantity of the ice-trace compartments in the solids were obtained from the smaller field-of-view data set. Five cross-sectional 2D images at equally spaced planes (approximately

100- $\mu\text{m}$  distance) of the small solids, viewed from each of three angles (XY, XZ, YZ), were used to obtain the number of compartments in each circular area (1-mm diameter).

### Thermal Analysis of Frozen Solutions and Freeze-Dried Solids

Thermal analysis of the frozen solutions and the freeze-dried solids were performed using a differential scanning calorimeter (DSC Q-10, TA Instruments, New Castle, DE). Aqueous solutions (10  $\mu\text{L}$ ) in hermetic aluminum cells were cooled from room temperature to  $-70^\circ\text{C}$  at  $10^\circ\text{C}/\text{min}$  before we performed a heating thermal scan at  $5^\circ\text{C}/\text{min}$ . Thermal properties of lyophilized solids (1–2 mg) were obtained by scanning the solid-containing cells from  $-10$  to  $240^\circ\text{C}$  at  $10^\circ\text{C}/\text{min}$ .

### Scanning Electron Microscopy Analysis

We studied the morphological features of freeze-dried solids using SEM (JSM-6320F, JEOL, Tokyo, Japan) at the Hanaichi Ultrastructure Research Institute Co. (Okazaki, Japan). Prior to imaging, sliced solid samples were coated with osmium, and the samples were exposed to a 5-kV acceleration voltage.

### Measurement of Residual Water Content

A CA-200 Karl Fischer coulometric titrator (Mitsubishi Chemical Analytech Co., Chigasaki, Japan) was used to determine the amount of water in the freeze-dried solids after they were suspended in dehydrated methanol.

## RESULTS

Lyophilization of the aqueous solutions containing a protein (rHA), trehalose, and sodium phosphate buffer after each of the four freezing methods resulted in the cylindrical micro-porous solids that had not physically collapsed (e.g., bubbling or shrinking). Some solids obtained upon drying of the  $\text{LN}_2$ -frozen solutions showed radial cracks. Karl Fischer measurements showed low residual water content ( $<0.5\%$ , *w/w*) in these solids. In addition, thermal analysis of the frozen solutions and the dried solids showed a  $T_g'$  of  $-29.3 \pm 0.2^\circ\text{C}$  and a glass transition temperature ( $T_g$ ) at above  $70^\circ\text{C}$ , respectively (data not shown). These high transition temperatures explain the structural integrity of the freeze-dried solids prepared at the lower shelf temperature during the primary drying step ( $-32^\circ\text{C}$ ).

Figure 1 shows X-ray micro-CT and SEM images of the solids that were dried after immersing the samples in liquid nitrogen. The  $\text{LN}_2$ -freezing induced ice growth from the

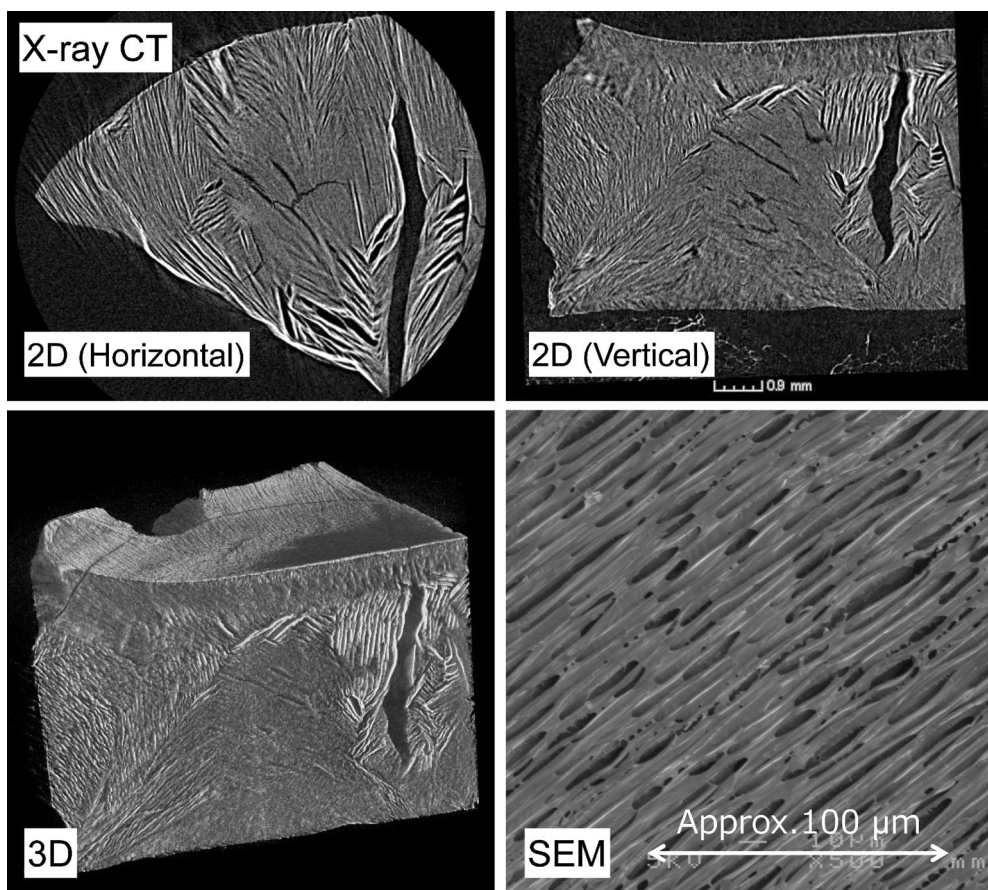


**Fig. 1.** The X-ray micro-CT and SEM images of a quarter-sized piece of a lyophilized solid containing rHA, trehalose, and sodium phosphate buffer. An aqueous solution in flat-bottom glass tube was frozen by immersion in liquid nitrogen before drying under vacuum

interface contacting the tubes (directional solidification) (34). The white areas in the 2D and 3D CT images indicate solid regions, while the dark areas inside the solid represent the pores left after ice sublimation (20). The big black space inside the solid should indicate a large crack. The solids showed fibrous or tubular local morphology and traces of linear ice, confirming the advancing ice growth. Some horizontal cross-sectional 2D images suggest that a crack forms at the boundary of the ice grown from different points. The SEM image of the solid supported these observations.

Figure 2 shows the X-ray micro-CT 2D images of the solids that were dried after freezing of the aqueous solutions by several methods. The analysis gave multiple digitally sliced horizontal (XY, circular) and vertical (XZ, YZ, rectangular) cross-sectional images. All the solids dried after the shelf-ramp cooling, post-freeze heat treatment, or the controlled nucleation showed traces of dispersing small particulate ice in the horizontal (middle height) and vertical (center)

sections, which is typical in suspension freezing. The variations in the pore structure of the cakes indicated different ice crystal morphologies that depended on the preparation methods. The solid obtained from conventional shelf-ramp freezing showed uniform fine pores in the horizontal section images and a higher-density upper surface layer in the vertical section images. No apparent precipitated components were observed at the bottom of the cake. An air view 3D image of the solid indicated traces of needle-like ice crystals lying parallel and horizontal in the upper surface (Fig. 3).

The solids dried after the post-freeze heat treatment and the controlled nucleation both showed horizontal section 2D images that suggested coarse microporous structure compared to those of the conventional shelf-frozen dried solids (Fig. 2). These solids also showed the higher-density upper surface layer. The controlled nucleation induced a fuzzy local texture with traces of parallel rectangular ice crystals running vertically in the upper center of the solid in the vertical section

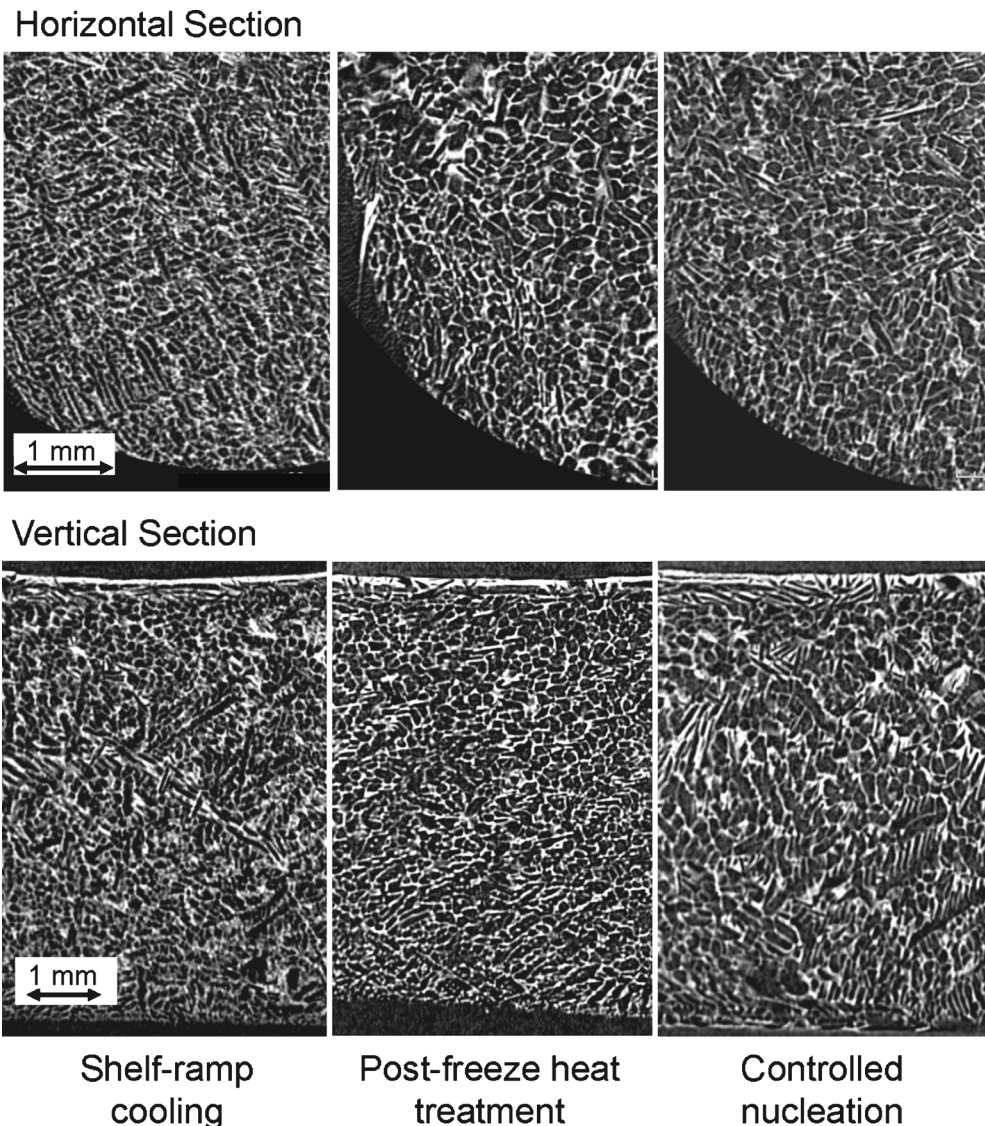


**Fig. 2.** Horizontal and vertical section of X-ray 2D micro-CT images of freeze-dried solids containing rHA, trehalose, and sodium phosphate buffer. The solids were dried after shelf-ramp freezing, post-freeze heat treatment, or freezing by controlled nucleation

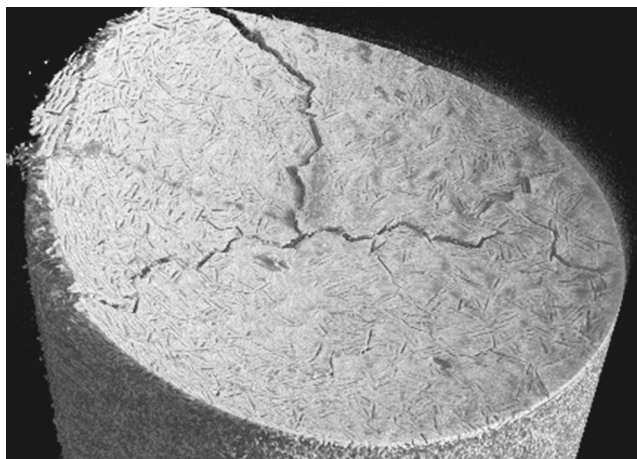
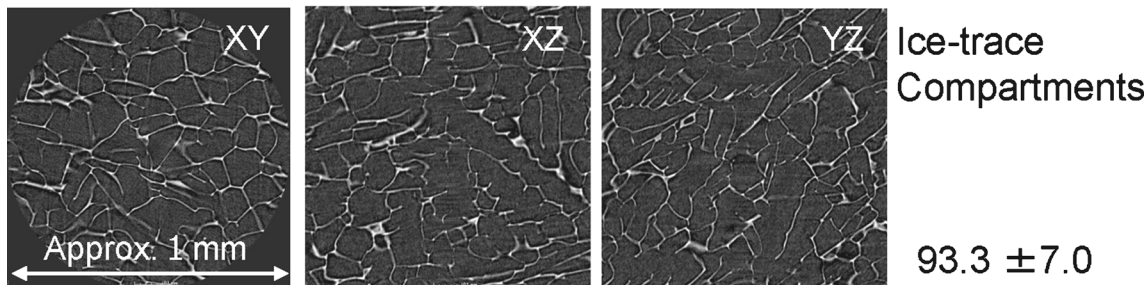


**Fig. 3.** An air view of 3D micro-CT image showing the upper surface of a freeze-dried solid containing rHA, trehalose, and sodium phosphate buffer obtained by drying of a post-freeze heat-treated solution

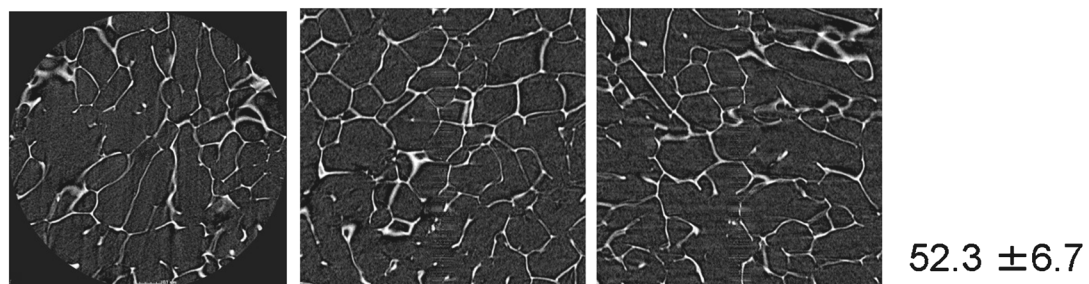
micro-CT image. This particular morphology should be explained by the ice formation and growth from top of the solutions (16). The freeze-induced solutions remained slushy and translucent for 20–30 min near the equilibrium freezing temperature (−5 to 0°C) before they became opaque and white after they completed the liquid-to-solid phase transition (data not shown) (6).

The X-ray micro-CT analysis was also performed to study the local structure of the dried solids more precisely. Figures 4 and 5 show the smaller-scale 2D and 3D X-ray micro-CT images and the SEM images of the solids prepared from inside of the cylindrical lyophilized cakes. They clearly show an architecture consisting of wall-like solids surrounding traces of each ice crystal. Most of the ice crystal traces were shaped like irregular rectangles rather than simple spheres or cubes. Preparation of cubic samples made their original direction unclear in the smaller-scale images. The reconstructed 3D images showed solid morphologies that were comparable with those found in the SEM observation (Fig. 5).

#### Shelf-ramp cooling



#### Post-freeze heat treatment



#### Controlled nucleation

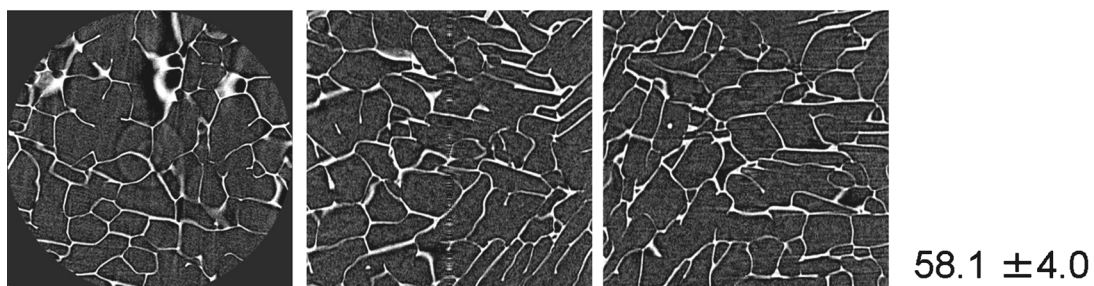


**Fig. 4.** The small field-of-view X-ray micro-CT 2D images of freeze-dried solids containing rHA, trehalose, and sodium phosphate buffer. The solutions were dried after the original solutions were frozen by shelf-ramp cooling, post-freeze heat treatment, or by controlled nucleation. Number of ice-trace compartments in 15 2D images (circular area, 1-mm diameter) of the particular solids was also included (average  $\pm$  s.d.)

The smaller-scale 2D image also showed reduced number of ice-trace compartments in the solids obtained after the post-freeze heat treatment and the controlled nucleation, indicating larger ice-trace pore compartments (Fig. 4). The post-freeze heat-treated dried solid showed larger variation in the width of lines between the ice-trace compartments. Many small holes in the SEM image suggested uneven thicknesses of the walls. The controlled nucleation during the freezing step resulted in the solids that were composed of relatively thick and uniform walls, as observed through the X-ray micro-CT and SEM images (19). The observation was in agreement with reduced specific surface area (14) reported in the solids obtained after some controlled nucleation methods. It may take longer time to remove unfrozen water from the thick walls during the secondary drying segment (4).

## DISCUSSION

The X-ray micro-CT analysis provided 2D and 3D images of microporous freeze-dried solids, which mimic therapeutic protein formulations, at much higher resolutions than previous studies have achieved (20,27). Some micro-CT images, which were obtained with reasonable scan times, clearly indicated the structure of solid walls surrounding trace of each ice crystal. The structures were comparable with those observed in SEM images. Recent advances in the instruments, such as improvements in X-ray detection and rotation control, as well as advancements in data processing techniques will continue to improve this analysis method (31–33). Overall, the X-ray micro-CT and SEM analysis would provide complimentary morphological information for lyophilized pharmaceuticals, which is important in the formulation and process optimization steps of these products.

The X-ray micro-CT analysis requires only simple sample preparation and provides a significant amount of morphological information. The method provides the larger field-of-view images without physically slicing the hygroscopic freeze-dried solids, which often alters their surface structures before the SEM analysis (20). Obtaining some smaller field-of-view images should require preparation of the smaller solids to reduce the distance between the X-ray source and the sample on the rotating stage. The preparation should give larger effect on the surface structure (e.g., SEM) compared to the microporous morphology inside of the solid (micro-CT). Contrarily, the SEM analysis should have some advantages in its wider availability, clear images, and established processing methods. Flat-bottom tubes were used to obtain intact cylindrical freeze-dried cakes in this study. It is often difficult to remove the cakes from lyophilization vials without disrupting them. However, analysis of appropriate smaller portions would provide sufficient morphological information, specifically regarding the ice crystal structures. Availability of overall and local solid morphology at arbitrary positions within the solids should significantly increase our ability to identify regional variations, including the ice crystal patterns, occurrence of local collapses, and uneven distribution of ingredients (e.g., solid precipitation, dense surface layer). This structural 3D data may also lead to the development of logical and/or mathematical descriptions of water vapor escape, which would enable further optimization of the freeze-drying processes (22).

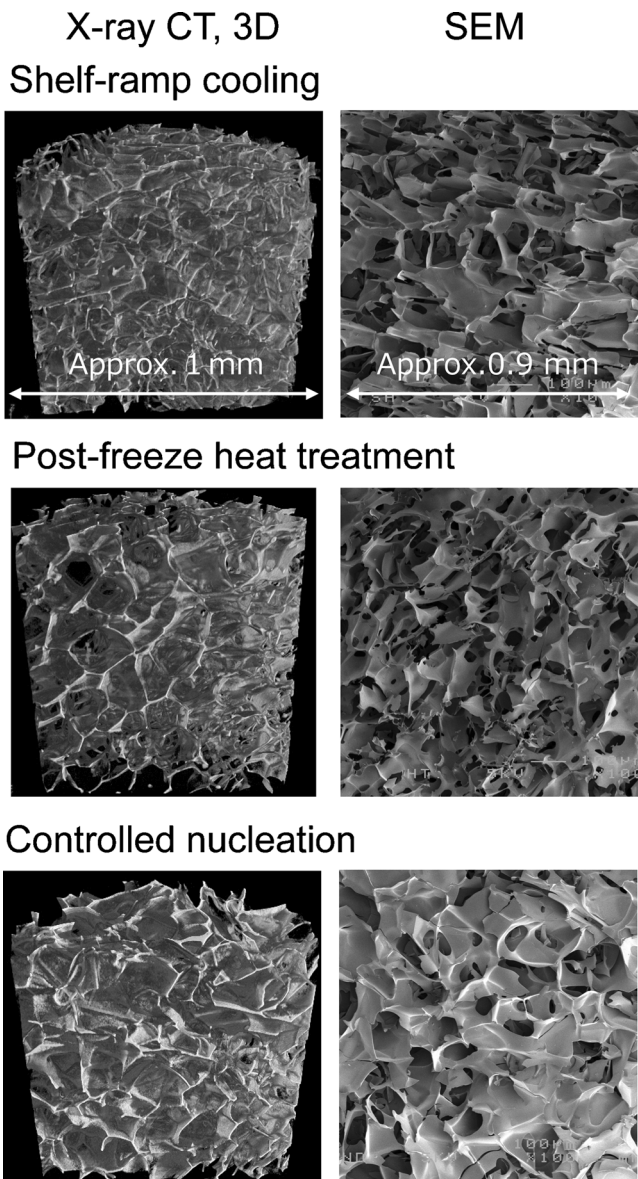


**Fig. 5.** The small field-of-view X-ray micro-CT 3D images and SEM images of lyophilized solids containing rHA, trehalose, and sodium phosphate buffer dried after freezing by several methods

The X-ray micro-CT images clearly indicated the variations in the local structure of the solids obtained after the different freezing methods. The solids dried after the post-freeze heat treatment and the controlled nucleation showed traces of larger ice crystals compared to the shelf-frozen dried solids. The post-freeze heat treatment induces Ostwald ripening of ice crystals and concomitant structural changes in the surrounding concentrated solute phase. The formation of larger pores, as a result of the larger ice crystal, and their increased connectivity should allow faster transition of water vapor during the primary and secondary drying steps. Among many reported controlled nucleation methods available, the depressurization and quick release method was chosen to induce ice formation because of its applicability in standard laboratory lyophilizers (6,18). Evaporation-induced cooling of

the solution surface and induction of small ice crystals that are blown from the condenser by the nitrogen gas flow are considered to trigger the simultaneous freezing in many tubes. Other controlled nucleation methods are preferred for sterile freeze-drying in production-scale lyophilizers. Possible differences in the extent of supercooling, the speed of ice crystal growth, and thermal histories that arise from different controlled nucleation methods should affect the architecture of the resulting ice crystals.

## CONCLUSION

The results of this study indicate relevance of 3D X-ray micro-CT as a method to be used for characterizing the morphology of freeze-dried solids. This technique allows for simple sample preparation, involves a short measurement time, and provides structural information at all the positions within the solids. All of these characteristics represent advantages over conventional methods for studying morphology. The micro-CT imaging was capable of detecting structural differences in each ice crystal traces that were formed under different freezing conditions. The structural information should assist formulation and process developments.

## ACKNOWLEDGMENTS

This study was supported partially by Japan Health Labour Sciences Research Grant. We thank Mr. Horiuchi (Yamato Scientific Co.) and Dr. Hanaoka (Microscopic Scan Co.) for technical supports.

## REFERENCES

1. Nail SL, Jiang S, Chongprasert S, Knopp SA. Fundamentals of freeze-drying. *Pharm Biotechnol*. 2002;14:281–360.
2. Akers MJ, Vasudevan V, Stickelmeyer M. Formulation development of protein dosage forms. *Pharm Biotechnol*. 2002;14:47–127.
3. Tang X, Pikal MJ. Design of freeze-drying processes for pharmaceuticals: practical advice. *Pharm Res*. 2004;21:191–200.
4. Geidobler R, Konrad I, Winter G. Can controlled ice nucleation improve freeze-drying of highly-concentrated protein formulations? *J Pharm Sci*. 2013;102:3915–9.
5. Colandene JD, Maldonado LM, Creagh AT, Vrettos JS, Goad KG, Spitznagel TM. Lyophilization cycle development for a high-concentration monoclonal antibody formulation lacking a crystalline bulking agent. *J Pharm Sci*. 2007;96:1598–608.
6. Geidobler R, Winter G. Controlled ice nucleation in the field of freeze-drying: fundamentals and technology review. *Eur J Pharm Biopharm*. 2013;85:214–22.
7. Kasper JC, Pikal MJ, Friess W. Investigations on polyplex stability during the freezing step of lyophilization using controlled ice nucleation—the importance of residence time in the low-viscosity fluid state. *J Pharm Sci*. 2013;102:929–46.
8. Konstantinidis AK, Kuu W, Otten L, Nail SL, Sever RR. Controlled nucleation in freeze-drying: effects on pore size in the dried product layer, mass transfer resistance, and primary drying rate. *J Pharm Sci*. 2011;100:3453–70.
9. Rambhatla S, Ramot R, Bhugra C, Pikal MJ. Heat and mass transfer scale-up issues during freeze drying: II. Control and characterization of the degree of supercooling. *AAPS PharmSciTech*. 2004;5:54–62.
10. Searles JA, Carpenter JF, Randolph TW. Annealing to optimize the primary drying rate, reduce freezing-induced drying rate heterogeneity, and determine  $T_g'$  in pharmaceutical lyophilization. *J Pharm Sci*. 2001;90:872–87.
11. Cavatur RK, Suryanarayanan R. Characterization of frozen aqueous solutions by low temperature X-ray powder diffractometry. *Pharm Res*. 1998;15:194–9.
12. Nakagawa K, Hottot A, Vessot S, Andrieu J. Influence of controlled nucleation by ultrasounds on ice morphology of frozen formulations for pharmaceutical proteins freeze-drying. *Chem Eng Process*. 2006;45:783–91.
13. Passot S, Tréléa IC, Marin M, Galan M, Morris GJ, Fonseca F. Effect of controlled ice nucleation on primary drying stage and protein recovery in vials cooled in a modified freeze-dryer. *J Biomech Eng*. 2009;131:074511.
14. Patel SM, Bhugra C, Pikal MJ. Reduced pressure ice fog technique for controlled ice nucleation during freeze-drying. *AAPS PharmSciTech*. 2009;10:1406–11.
15. Bhatnagar BS, Pikal MJ, Bogner RH. Study of the individual contributions of ice formation and freeze-concentration on isothermal stability of lactate dehydrogenase during freezing. *J Pharm Sci*. 2008;97:798–814.
16. Kramer M, Sennhenn B, Lee G. Freeze-drying using vacuum-induced surface freezing. *J Pharm Sci*. 2002;91:433–43.
17. Fernandez PP, Otero L, Guignon B, Sanz PD. High-pressure shift freezing versus high-pressure assisted freezing: effects on the microstructure of a food model. *Food Hydrocolloids*. 2006;20:510–22.
18. Geidobler R, Mannschedel S, Winter G. A new approach to achieve controlled ice nucleation of supercooled solutions during the freezing step in freeze-drying. *J Pharm Sci*. 2012;101:4409–13.
19. Awotwe-Otoo D, Agarabi C, Read EK, Lute S, Brorson KA, Khan MA, et al. Impact of controlled ice nucleation on process performance and quality attributes of a lyophilized monoclonal antibody. *Int J Pharm*. 2013;450:70–8.
20. Parker A, Rigby-Singleton S, Perkins M, Bates D, Le Roux D, Roberts CJ, et al. Determination of the influence of primary drying rates on the microscale structural attributes and physicochemical properties of protein containing lyophilized products. *J Pharm Sci*. 2010;99:4616–29.
21. Lam P, Patapoff TW. An improved method for visualizing the morphology of lyophilized product cakes. *PDA J Pharm Sci Tech*. 2011;65:425–43.
22. Overcahier DE. Microscopy of lyophilized proteins. In: Costantino HR, Pikal MJ, editors. *Lyophilization of biopharmaceuticals*. Arlington: AAPS; 2004. p. 337–63.
23. Hottot A, Vessot S, Andrieu J. A direct characterization method of the ice morphology. Relationship between mean crystals size and primary drying times of freeze-drying processes. *Drying Tech*. 2004;22:2009–21.
24. Appoloni CR, Macedo Á, Fernandes CP, Philippi PC. Characterization of porous microstructure by x-ray microtomography. *X-Ray Spectrom*. 2002;31:124–7.
25. Fu X, Elliott JA, Benthall AC, Hancock BC, Cameron RE. Application of X-ray microtomography and image processing to the investigation of a compacted granular system. *Part Part Syst Charact*. 2006;23:229–36.
26. Wray P, Chan KLA, Kimber J, Kazarian SG. Compaction of pharmaceutical tablets with different polymer matrices studied by FTIR imaging and X-ray microtomography. *J Pharm Sci*. 2008;97:4269–77.
27. Mousavi R, Miri T, Cox PW, Fryer PJ. A novel technique for ice crystal visualization in frozen solids using X-ray micro-computed tomography. *J Food Sci*. 2005;70:e437–42.
28. Mousavi R, Miri T, Cox PW, Fryer PJ. Imaging food freezing using X-ray microtomography. *Int J Food Sci Tech*. 2007;42:714–27.
29. Nygaard JV, Andersen MØ, Howard KA, Foss M, Bunger C, Kjems J, et al. Investigation of particle-functionalized tissue engineering scaffolds using X-ray tomographic microscopy. *Biotechnol Bioeng*. 2008;100:820–9.
30. Xiao X, Tao LR, Hua TC. Micro-computed tomography observation of sublimation interface and image analysis on sublimation process during freeze-drying. *Cryo Lett*. 2007;28:253–60.
31. Dorsey SM, Lin-Gibson S, Simon CGJ. X-ray microcomputed tomography for the measurement of cell adhesion and proliferation in polymer scaffolds. *Biomaterials*. 2009;30:2967–74.

32. Miyoshi M, Hamakubo T, Kodama T, Tsuchiya M, Koishikawa A, Aoki N. Development of the low-energy soft x-ray CT instrument for the soft material structural analysis. *J Vac Sci Technol*. 2008;B26:2356–61.
33. Mizutani R, Suzuki Y. X-ray microtomography in biology. *Micron*. 2012;43:104–15.
34. Petzold G, Aguilera JM. Ice morphology: fundamentals and technological applications in foods. *Food Biophys*. 2009;4:378–96.